Giant Optical Nonlinearity of Graphene in a Strong Magnetic Field

Xianghan Yao and Alexey Belyanin

Phys. Rev. Lett. **108**, 255503 — Published 21 June 2012

DOI: 10.1103/PhysRevLett.108.255503

Giant optical nonlinearity of graphene in a strong magnetic field

Xianghan Yao[1] and Alexey Belyanin[1,*]

[1]*Department of Physics and Astronomy, Texas A&M University, College Station, TX, 77843 USA*

(Dated: 20 October 2011)

We calculate the nonlinear optical response of graphene in strong magnetic and optical fields, using quantum-mechanical density-matrix formalism. We show that graphene in a magnetic field possesses a giant mid/far-infrared optical nonlinearity, perhaps the highest among known materials. The high nonlinearity originates from unique electronic properties and selection rules near the Dirac point. As a result, even one monolayer of graphene gives rise to appreciable nonlinear frequency conversion efficiency for incident infrared radiation.

PACS numbers: 81.05.ue, 42.65.-k

Graphene, a two-dimensional monolayer of carbon atoms arranged in a hexagonal lattice, holds many records as far as its mechanical, thermal, electrical, and optical properties are concerned; see. e.g. [1] for the review. With this Letter we would like to add yet another distinction to this list of superlatives: we show that graphene in a strong magnetic field has a giant infrared optical nonlinearity, the highest of all materials we know.

Strong optical nonlinearity of graphene, like most of its unique electrical and optical properties, stems from linear energy dispersion of carriers near the K,K' points of the Brillouin zone. As a result, the electron velocity induced by an incident electromagnetic wave is a nonlinear function of induced electron momentum. Nonlinear electromagnetic response of classical charges with linear energy dispersion has been studied theoretically in [2]. Recently, four-wave mixing in mechanically exfoliated graphene flakes without magnetic field has been observed at near-infrared wavelengths [3]. Effective bulk third-order susceptibility was estimated to have a very large value, $\chi^{(3)} \sim 10^{-7}$ esu, which is more than an order of magnitude larger than in gold films.

Nonlinear cyclotron resonance in graphene was considered theoretically in [4], again in the classical limit, by solving the equation of motion $\mathbf{F} = d\mathbf{p}/dt$ for a massless charge. Classical approximation can be applied to electrons in low magnetic field that are occupying highly excited Landau levels $n \gg 1$, when energy and momentum quantization are neglected. Here we present rigorous quantum mechanical description of the nonlinear optical response of graphene, which is valid for quantizing magnetic fields and strong optical fields, including the effect of saturation of inter-Landau level transitions. Due to unique optical selection rules for "massless" electrons near the Dirac point, one can implement a four-wave mixing interaction in which all optical fields are resonant to allowed optical transitions. The resulting magnitude of $\chi^{(3)}$ turns out to be astonishingly large, of the order of 0.1 esu at mid/far-infrared wavelengths in the field of several Tesla. This leads to the nonlinear signal intensity of the order of 10 W/cm^2 per monolayer for incident field intensity close to the optical saturation.

Graphene in a magnetic field can be compared with coupled quantum well heterostructures, where one can also achieve fully resonant nonlinear optical interaction involving a cascade of allowed intersubband transitions, similarly to Fig. 1b; see e.g. [5–8]. The predicted magnitude of $\chi^{(3)}$ in magnetized graphene is still many orders of magnitude higher than the reported third-order resonant intersubband nonlinearity $\chi^{(3)} \sim 7\times10^{-8}$ esu in the mid-infrared range for quantum cascade laser structures [6], although the latter number could be made higher by increasing doping. Other materials with non-parabolic energy dispersion of electrons, showing strong optical nonlinearity in the mid/far-infrared range, include narrow gap semiconductors [9] and semiconductor superlattices [10]. In both cases, the maximum predicted or measured $\chi^{(3)}$ was of the order of 10^{-9} esu.

Linear (one-photon) absorption in monolayer and bilayer graphene in strong magnetic fields has been calculated in [11] using Keldysh Green's function formalism. This approach is inconvenient when it comes to calculating the nonlinear optical response. The density matrix formalism adopted in this paper provides a rigorous, intuitive, and straightforward framework for calculating the hierarchy of nonlinear optical susceptibilities and interaction of strong multi-frequency EM fields or ultrashort pulses with graphene. Expressions for one-photon absorbance obtained in [11] can be retrieved by calculating the linear susceptibility in the limit of a weak monochromatic field.

In the absence of the optical field, the effective-mass Hamiltonian [12–14] for a graphene monolayer (in the xy plane) in the magnetic field $B\hat{z}$, in the vicinity of K and K' points [15] in the nearest-neighbor tight-binding model is given by

$$\hat{H}_0 = \upsilon_F \begin{pmatrix} 0 & \hat{\pi}_x - i\hat{\pi}_y & 0 & 0 \\ \hat{\pi}_x + i\hat{\pi}_y & 0 & 0 & 0 \\ 0 & 0 & 0 & \hat{\pi}_x + i\hat{\pi}_y \\ 0 & 0 & \hat{\pi}_x - i\hat{\pi}_y & 0 \end{pmatrix} \tag{1}$$

where υ_F is a band parameter (10^8 cm/s) [16, 17], $\hat{\vec{\pi}} = \hat{\vec{p}} + e\vec{A}/c$, $\hat{\vec{p}}$ is the electron momentum operator, and $\vec{A}$

is the vector potential, which is equal to $(0, Bx)$ here.

To simplify notations, we write down the solutions to the Schrödinger equation $\hat{H}_0\Psi = \varepsilon\Psi$ separately near the K and K' point. For example, near the K point the Hamiltonian is $\hat{H}_0 = \upsilon_F\vec{\sigma}\cdot\vec{\pi}$, where $\vec{\sigma} = (\sigma_x, \sigma_y)$ is a vector of Pauli matrices. The eigenfunction is specified by two quantum numbers, n and k_y, where $n = 0, \pm1, \pm2, \cdots$, and k_y is the electron wave vector along y direction [13]:

$$\Psi_{n,k_y}(r) = \frac{C_n}{\sqrt{L}}\exp(-ik_y y)\begin{pmatrix} \mathrm{sgn}(n) i^{|n|-1}\phi_{|n|-1} \\ i^{|n|}\phi_{|n|} \end{pmatrix} \quad (2)$$

with $C_n = 1$ when $n = 0$, $C_n = 1/\sqrt{2}$ when $n \neq 0$, and

$$\phi_{|n|} = \frac{H_{|n|}\left((x - l_c^2 k_y)/l_c\right)}{\sqrt{2^{|n|}|n|!\sqrt{\pi}l_c}}\exp\left[-\frac{1}{2}\left(\frac{x - l_c^2 k_y}{l_c}\right)^2\right],$$

where $l_c = \sqrt{c\hbar/eB}$ and $H_n(x)$ is the Hermite Polynomial. The eigen energy is $\varepsilon_n = \mathrm{sgn}(n)\hbar\omega_c\sqrt{|n|}$, where $\omega_c = \sqrt{2}\upsilon_F/l_c$.

In the presence of the incident classical optical field $\vec{E} = (1/2)\hat{e}E_\omega e^{-i\omega t}$ polarized along the vector $\hat{e}$ in the x-y plane ($\hat{e}_{LHS} = [\hat{x} - i\hat{y}]/\sqrt{2}$ and $\hat{e}_{RHS} = [\hat{x} + i\hat{y}]/\sqrt{2}$, which denote left-hand and right-hand circularly polarized light), we add the vector potential of incident optical field, $\vec{A}_{opt} = ic\vec{E}/\omega$, to the vector potential of the magnetic field in the generalized momentum operator $\hat{\vec{\pi}}$ in the Hamiltonian. This results in adding the interaction Hamiltonian $\hat{H}_{int}$ to $\hat{H}_0$, where

$$\hat{H}_{int} = \upsilon_F\vec{\sigma}\cdot\frac{e}{c}\vec{A}_{opt} \quad (3)$$

This linear in $\vec{A}_{opt}$ expression for the interaction Hamiltonian is exact for the Hamiltonian in Eq. (1), unlike the case of the kinetic energy operator quadratic in momentum, where the term proportional to A_{opt}^2 is usually neglected. Note also that Eq. (3) does not contain the momentum operator and its matrix elements are simply determined by the matrix elements of $\vec{\sigma}$. This immediately gives the selection rules [11] for the transitions between the LLs: $\hat{e}_{LHS}$ photons are absorbed when $|n_f| = |n_i| + 1$, whereas $\hat{e}_{RHS}$ photons are absorbed when $|n_f| = |n_i| - 1$. Here n_i and n_f indicate initial and final energy quantum numbers of LLs.

Now we can write a standard time-evolution equation for the density matrix of Dirac electrons in graphene coupled to an arbitrary optical field:

$$\frac{\partial\hat{\rho}}{\partial t} = -\frac{i}{\hbar}[\hat{H}_0 + \hat{H}_{int}, \hat{\rho}] + \hat{R}(\hat{\rho}). \quad (4)$$

Here $\hat{R}(\hat{\rho})$ describes incoherent relaxation due to disorder, interaction with phonons, and many-body carrier-carrier interactions. Equations Eq. (4) have to be solved together with Maxwell's equations that contain the optical polarization $\vec{P}(\vec{r}, t) = (1/V)\mathrm{Tr}(\hat{\rho}\cdot\vec{\mu})$ (average dipole moment $\langle\vec{\mu}\rangle$ per unit volume) as a source term. In the perturbative regime, they give rise to the hierarchy of the optical susceptibilities $\chi^{(n)}$, but they are also valid for describing non-perturbative coupling to strong fields, interaction with ultrashort pulses etc.

Since graphene is essentially a 2D system, it makes sense to introduce a surface (2D) polarization P_s determined as an average dipole moment per unit area rather than unit volume.

For a weak monochromatic field one can retain only the term $\rho_{mn}^{(1)} = (\rho_{nn}^{(0)} - \rho_{mm}^{(0)})\langle m|\hat{H}_{int}|n\rangle/(\varepsilon_m - \varepsilon_n - \hbar\omega - i\hbar\gamma_{mn})$ linear with respect to the field and take the sum $\sum_{m,n}\rho_{nm}\vec{\mu}_{mn}$ to obtain an expression for the linear susceptibility:

$$\chi^{(1)}(\omega) = \sum_{n\geq1;\alpha,\alpha'}\frac{2C_{n-1}^2 e^2\upsilon_F^2}{\pi l_c^2\hbar\omega\omega_c(\alpha\sqrt{n} - \alpha'\sqrt{n-1})} \times\frac{(\nu_{n,\alpha} - \nu_{n-1,\alpha'})}{(\alpha'\sqrt{n-1}\omega_c - \alpha\sqrt{n}\omega_c - \omega - i\gamma)}. \quad (5)$$

Here we used $\langle m|\hat{H}_{int}|n\rangle = -(i/\omega)e\upsilon_F\langle m|\vec{\sigma}|n\rangle\vec{E}(\omega)$ and $\langle m|\vec{\mu}|n\rangle = (i\hbar/(\varepsilon_n - \varepsilon_m))e\upsilon_F\langle m|\vec{\sigma}|n\rangle$. Note that the matrix element of the interaction Hamiltonian can be written as $-\tilde{\vec{\mu}}_{mn}\vec{E}$, where $\tilde{\vec{\mu}}_{mn} = (i/\omega)e\upsilon_F\langle m|\vec{\sigma}|n\rangle$, and $\tilde{\vec{\mu}}_{mn} = \vec{\mu}_{mn}$ when $\varepsilon_n - \varepsilon_m = \hbar\omega$.

We assumed for simplicity that the relaxation term for the off-diagonal density matrix elements $R_{mn} = -\gamma_{mn}\rho_{mn}$ and all γ's are the same. For easy comparison, we used the same notations for LLs as in [11]: $\alpha, \alpha' = \pm$ denote whether the corresponding state belongs to the conduction (+) or valence (-) band and $\nu_{n,\alpha}$ are the filling factors of LLs; a complete occupation corresponds to $\nu = 2$. The degeneracy of a given LL is $2/(\pi l_c^2)$ including both spin and valley degeneracy. After calculating the dimensionless linear absorbance as $(2\pi\omega/c)\mathrm{Im}[\chi^{(1)}(\omega)]$ we obtain the same result as in [11].

Now we consider a specific example of the nonlinear optical interaction, namely the four-wave mixing. Consider a strong bichromatic field $\vec{E} = (1/2)(\vec{E}_1\exp(-i\omega_1 t) + \vec{E}_2\exp(-i\omega_2 t) + \mathrm{c.c.})$ normally incident on the graphene layer. Here ω_1 is nearly resonant with the transition from $n = -1$ to $n = 2$ and $\vec{E}_1$ has left circular polarization. The frequency ω_2 is nearly resonant with the transition from $n = 0$ to $n = \pm1$ and $\vec{E}_2$ has linear polarization, so that it couples both to transition $-1 \to 0$ and $0 \to 1$, as shown in Fig. 1. As a result of the four-wave mixing interaction, the right-circularly polarized field $\vec{E}_3$ at frequency $\omega_3 = \omega_1 - 2\omega_2$ nearly resonant with the transition from $n = 2$ to $n = 1$ is generated.

Efficient nonlinear mixing becomes possible due to unique selection rules $\Delta|n| = \pm1$ which enable transitions with change in n greater than 1, for example the transition from state $n = -1$ to state $n = 2$. This transition would be forbidden in conventional LL systems with $\Delta n = \pm1$ selection rule. The effective dipole moments for

all transitions shown in Fig. 1b scale as v_F/ω, i.e. they are similar to each other within a factor of 2 and are very large: of the order of 10-100 $\mathring{A}$ in the mid/far-IR range. This, in combination with sharp peaks in the density of states at LLs gives a strong nonlinear response.

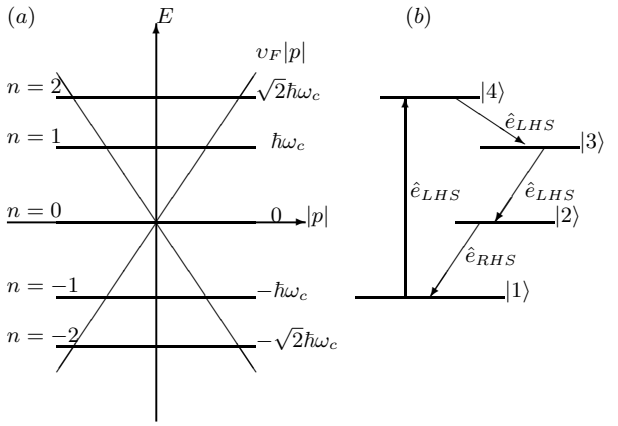

FIG. 1: (a): Landau levels near the K point superimposed on the electron dispersion without magnetic field $E = \pm v_F|p|$. (b): A scheme of resonant four-wave mixing process in the four-level system of LLs with energy quantum numbers $n = -1, 0, +1, +2$. The case of exact resonance is shown. Polarization of light corresponds to the allowed transitions.

Since LLs are not equidistant, we can assume that the optical fields interact resonantly only with states $n = -1, 0, 1, 2$, which we renamed to $n = 1, 2, 3, 4$ in Fig. 1b. The Hamiltonian can be truncated to a 4x4 matrix, where $(H_0)_{mn}$ is diagonal, with diagonal elements being the energies of corresponding LLs, and the interaction Hamiltonian is given by the matrix $-\tilde{\vec{\mu}}_{mn}\vec{E}$ as specified above. The resulting third-order nonlinear optical susceptibility at frequency $\omega_3 = \omega_1 - 2\omega_2$, defined as the ratio of the surface optical polarization $P(\omega_3) = (2/A)\mu_{34}\rho_{43}$ to the product of three fields $E_1(\omega_1)(E_2^*(\omega_2))^2$, is

$$\chi^{(3)}_{2D}(\omega_3) = \frac{-(2/\pi l_c^2)\mu_{34}\tilde{\mu}_{41}\tilde{\mu}_{32}\tilde{\mu}_{21}}{(i\hbar)^3\Gamma_{43}} \times\Bigg(-\frac{\rho_{33}-\rho_{22}}{\Gamma^*_{31}\Gamma^*_{32}} + \frac{\rho_{22}-\rho_{11}}{\Gamma^*_{31}\Gamma^*_{21}} + \frac{\rho_{44}-\rho_{11}}{\Gamma_{42}\Gamma_{41}} + \frac{\rho_{22}-\rho_{11}}{\Gamma_{42}\Gamma^*_{21}}\Bigg) \quad (6)$$

Here the complex linewidth factors in the weak-field limit are $\Gamma_{21} = \gamma_{21} + i((\varepsilon_2-\varepsilon_1)/\hbar-\omega_2)$, $\Gamma_{32} = \gamma_{32} + i((\varepsilon_3-\varepsilon_2)/\hbar-\omega_2)$, $\Gamma_{41} = \gamma_{41} + i((\varepsilon_4-\varepsilon_1)/\hbar-\omega_1)$, and $\Gamma_{43} = \gamma_{43} + i((\varepsilon_4-\varepsilon_3)/\hbar-\omega_3)$.

The third-order susceptibility as defined above is a function of the optical fields because the population differences decrease with increasing incident pump intensity due to the optical saturation (excitation of electrons to higher LLs), whereas the linewidth factor Γ_{43} increases with incident intensity (this is sometimes called power broadening). These dependences are quite cumbersome; to obtain a simple expression we assume that all fields are in exact resonance with corresponding transitions and all dephasing rates are the same, so that $\gamma_{mn} = \gamma$. The $\chi^{(3)}_{2D}$ depends on the incident fields only through dimensionless parameters $x = |E_1|/E^{\rm sat}_{14}$, $y = |E_2|/E^{\rm sat}_{12}$, where for a given transition $m \to n$ the saturation field at the line center is $E^{sat}_{mn} = \hbar\sqrt{\gamma/\tau_{mn}}/(2\mu_{mn})$ and τ_{mn} is the relaxation time of the population difference $\rho_{mm} - \rho_{nn}$ to the equilibrium in the absence of the optical fields. One can rewrite Eq. (6) as

$$\chi^{(3)}_{2D} \sim \frac{2\mu_{43}\tilde{\mu}_{41}\tilde{\mu}_{32}\tilde{\mu}_{21}f(x,y)}{\pi l_c^2(\hbar\gamma)^3} \sim \frac{3.7\times10^{-9}f(x,y)}{B(T)}\ \text{esu} \quad (7)$$

where the magnetic field $B(T)$ is expressed in Tesla, $f(x, y)$ is a dimensionless function of parameters x and y, and we took $\gamma = 3\times10^{13}$ s^{-1} for the dephasing rate in the numerical estimate [17]. For comparison, $\omega_c \simeq 10^{14}$ s^{-1} at $B = 3$ T.

When the incident fields are weak, $x, y \ll 1$, the populations are unperturbed. Assume for definiteness that state 1 is fully occupied while states 2,3, and 4 are empty, i.e. the Fermi level is between LLs $n = 0$ and $n = -1$. Then $f(x, y) = 3$. When x, y become much greater than 1, $f(x, y)$ decreases rapidly.

Equation (6) or (7) is a 2D (surface) susceptibility. To compare with bulk materials, we divide Eq. (7) by the monolayer thickness ~ 3 $\mathring{A}$ to obtain the bulk weak-field susceptibility $\chi^{(3)}_{3D} \sim 0.37\,(1/B(T))$ esu $= 5\times10^{-9}\,(1/B(T))\text{m}^2/\text{V}^2$. This is by far the strongest nonlinearity as compared to any material that we are aware of. Of course, bulk susceptibility does not make much sense if the sample consists of just one monolayer of graphene.

The frequencies involved in the four-wave mixing process fall into the mid/far-IR range for the magnetic field of a few Tesla, as shown in Fig. 2. In particular, at $B = 3$ T the generated nonlinear signal is at the wavelength of about 48 μm whereas the pump wavelengths are 8 and 20 μm.

From Maxwell's equations, the electric field amplitude $E_3(\omega_3)$ of the generated nonlinear signal is given by $E_3 = i(2\pi\omega_3/c)\chi^{(3)}_{2D}(\omega_3)E_1(E_2^*)^2$. The intensity of the nonlinear signal is

$$I_3(\omega_3) = \left(\frac{16\pi^2\omega_3}{c^2}\right)^2 |\chi^{(3)}_{2D}|^2 I_1(\omega_1)(I_2(\omega_2))^2. \quad (8)$$

For weak incident pump fields, when $x, y \ll 1$, $\chi^{(3)}$ does not depend on the pump fields and the power conversion efficiency of the nonlinear signal generation scales as $\sim 7\times10^{-5}(1/B(T))$ W/W^3 for the illuminated area

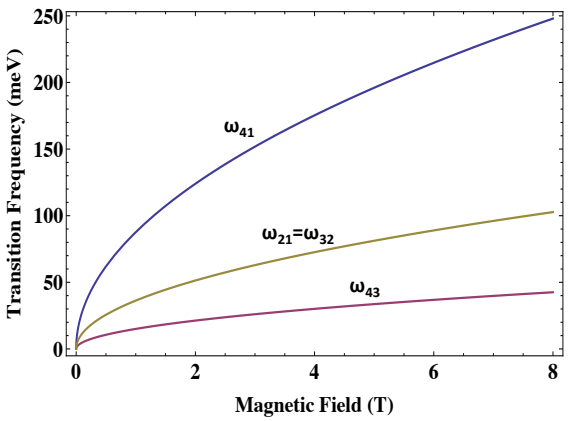

FIG. 2: Transition frequencies in the above 4-energy level graphene system. ω_{mn} indicates the transition frequency between level m and n.

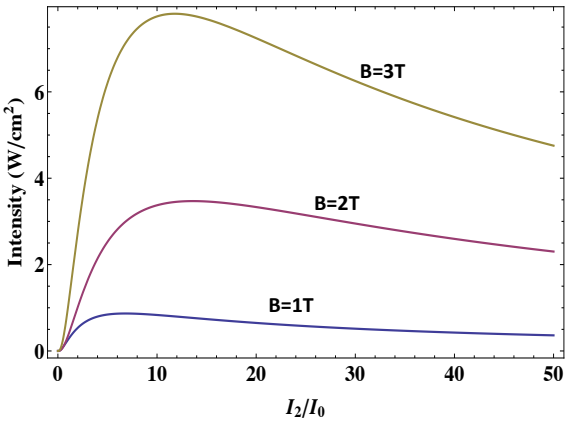

FIG. 3: Intensity of the 4-wave mixing signal as a function of the intensity of the pump field E_2 normalized by $I_0 = c|E_{\rm sat}|^2/8\pi \simeq 2.2\times10^5$ W/cm^2. The value of I_0 is the saturation intensity of the transition 1-2 calculated at $B = 1$ T and assuming that $1/\tau_{mn} = \gamma = 3\times10^{13}$ s^{-1}. I_1 is set to satisfy $y = 0.6x$.

$A = 10^{-4}$ cm^2. For strong incident fields above saturation, $x, y \gg 1$, the nonlinear signal intensity decreases due to the optical saturation and power broadening. The maximum intensity is reached at $x \simeq 2.6$ and $y \simeq 1.56$. Figure 3 shows the four-wave mixing signal intensity as a function of the pump intensity of the field E_2, whereas the second pump field is set to satisfy $y = 0.6x$, so that each curve goes through the maximum. The peak nonlinear signal intensity grows with the magnetic field as $\omega_3^2|\chi^{(3)}|^2|E_{\rm sat}|^6 \propto B^2$ because the saturation intensity $|E_{\rm sat}|^2$ scales as $1/\mu_{mn}^2 \propto B$. At $x \gg 1$ the nonlinear signal intensity drops as $1/x^2$.

The presented analysis becomes invalid for very high magnetic fields approaching ~ 100 T, when the highest frequency involved in the nonlinear mixing, $\omega_{41} \simeq 0.88$ eV. At these energies the deviation from linear electron dispersion, asymmetry between electrons and holes, and other effects related to interaction between distant neighbors in the lattice become significant [18]. In addition, spin splitting of the LLs becomes non-negligible (about 10 meV at 100 T) [19]. We also neglect many-body and excitonic effects.

In conclusion, graphene is a unique nonlinear-optical system in which the most fundamental properties that we take for granted are drastically modified. Graphene in a strong magnetic field possesses a very high infrared optical nonlinearity due to unique properties of quantized Landau levels near the Dirac point. The nonlinearity is expected to be ultrafast, enabling response to THz modulation. These properties of graphene may have important implications for coherent nonlinear generation and detection in the mid-infrared and THz range. One should expect to encounter similar unusual nonlinear optical properties in other materials which show a Dirac-cone dispersion, for example topological insulators and some high-T$_c$ superconductors [20, 21]. This could open interesting possibility of detection and control of topologically protected states by means of nonlinear optics.

This work was supported in part by NSF Grants OISE-0968405, EEC-0540832, and ECCS-0925446, and by the NHARP Project No. 003658-0010-2009.

* Electronic address: belyanin@tamu.edu

[1] K.S. Novoselov, Rev. Mod. Phys. 83, 837 (2011).

[2] S. A. Mikhailov and K. Ziegler, J. Phys.: Condens. Matter 20, 384204 (2008).

[3] E. Hendry, P.J. Hale, J. Moger, A.K. Savchenko, and S.A. Mikhailov, Phys. Rev. Lett. 105, 097401 (2010).

[4] S. A. Mikhailov, Phys. Rev. B 79, 241309(R) (2009).

[5] C. Gmachl, A. Belyanin, D.L. Sivco, Milton L. Peabody, N. Owschimikow, A. M. Sergent, F. Capasso, and A.Y. Cho, IEEE Journal of Quant. Electron., 39, 1345 (2003).

[6] T.S. Mosely, A. Belyanin, C. Gmachl, D.L. Sivco, M.L. Peabody, and A.Y. Cho, Optics Express 12, 2972 (2004).

[7] M. Troccoli, A. Belyanin, F. Capasso, E. Cubukcu, D. L. Sivco, and A.Y. Cho, Nature, 433, 845 (2005).

[8] M. Belkin, F. Capasso, A. Belyanin, D. L. Sivco, A. Y. Cho, D. C. Oakley, C. J. Vineis, and G. W. Turner, Nature Photonics, 1, 288 (2007).

[9] C. K. N. Patel, R. E. Slusher, and P. A. Fleury, Phys. Rev. Lett. 17, 1011 (1966).

[10] W. L. Bloss and L. Friedman, Appl. Phys. Lett. 41, 1023 (1982).

[11] D.S.L. Abergel and V. I. Fal'ko, Phys. Rev. B 75, 155430 (2007).

[12] T. Ando, J. Phys. Soc. Jpn. 74, 777 (2005).

[13] Y. Zheng and T. Ando, Phys. Rev. B 65, 245420 (2002).

[14] T. Ando, J. Phys. Soc. Jpn. 76, 024712 (2007).

[15] P. R. Wallace, Phys. Rev. 7, 622 (1947).

[16] Y. Zhang Y, Y-W. Tan, H.L. Stormer, and P. Kim, Nature 438, 201 (2005).

[17] Z. Jiang, E. A. Henriksen, L. C. Tung et al., Phys. Rev. Lett. 98, 197403 (2007).

[18] P. Venezuela, M. Lazzeri, and F. Mauri, Phys. Rev. B 84, 035433 (2011).

[19] Y. Zhang, Z. Jiang, J. P. Small, et al., Phys. Rev. Lett. 96, 136806 (2006).

[20] M. Koenig, S. Wiedmann, C. Bruene et al., Science 318, 766 (2007).

[21] P. Richard, K. Nakayama, T. Sato, et al., Phys. Rev. Lett. 104, 137001 (2010).